Experimental testing of a high-flux cavity receiver

John Pye, Joe Coventry, Felix Venn, José Zapata, Ehsan Abbasi, Charles-Alexis Asselineau, Greg Burgess, Graham Hughes, and Will Logie

Citation: AIP Conference Proceedings **1850**, 110011 (2017); doi: 10.1063/1.4984485

View online: http://dx.doi.org/10.1063/1.4984485

View Table of Contents: http://aip.scitation.org/toc/apc/1850/1

Published by the American Institute of Physics

Experimental Testing of a High-Flux Cavity Receiver

John Pye[1, a)], Joe Coventry[1], Felix Venn[1], José Zapata[1], Ehsan Abbasi[1], Charles-Alexis Asselineau[1], Greg Burgess[1], Graham Hughes[2] and Will Logie[1]

[1] *Solar Thermal Group, Research School of Engineering, Australian National University, Canberra, Australia.*
[2] *Faculty of Engineering, Imperial College, London, UK.*

[a)] Corresponding author: john.pye@anu.edu.au

Abstract. A new tubular cavity receiver for direct steam generation, 'SG4', has been built and tested on-sun based on integrated optical and thermal modelling. The new receiver achieved an average thermal efficiency of 97.1±2.1% across several hours of testing, and reduced the losses by more than half, compared to the modelled performance of the previous SG3 receiver and dish. Near-steady-state outlet steam temperatures up to 560°C were achieved during the tests.

INTRODUCTION

The 'SG4' Big Dish is a 500 m² paraboloidal dish concentrator designed for use in dish-Rankine arrays [1, 2], located on-site at the Australian National University (ANU). Although completed and first tested in 2009 (Figure 1), the original testing was conducted before a receiver had been designed to match the flux conditions of the new dish, and so the receiver from the earlier SG3 dish was mounted on SG4 for testing [3]. Poor-quality reflectometer equipment made it difficult to obtain an accurate receiver efficiency at the time, but the receiver thermal efficiency η_{th} (see below) of the SG3 receiver was estimated to be over 90%. The SG4 dish achieved excellent optical performance: its peak flux was 14,100 suns and its average concentration ratio was 2240 for 95% capture.

Recently, a project to design an optimised superheated direct steam generation tubular cavity receiver for the SG4 dish has been completed. The design was reported at SolarPACES 2015 [4]: results from an integrated optical and thermal model of the new design predicted a receiver thermal efficiency of 98.7% for an inlet/outlet temperature range of 60–500°C (Figure 1). The receiver has a single helical coil containing ~190 m of alloy 601H tube in ½-inch Sch. 40 and ¾-inch Sch. 40 sizes, with the larger pipe size being used for the superheated region, to reduce pressure drops. The predicted receiver efficiency is very high, when compared to the high-end values of 90% for the

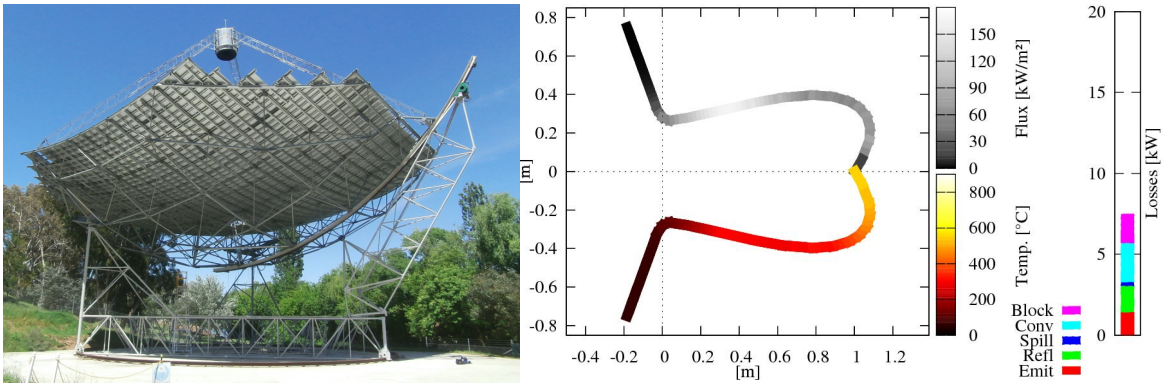

FIGURE 1. Left, the ANU 500 m² 'SG4' Big Dish, used for testing the new receiver [1]. Right, the cross-section, modelled flux and temperature profile and anticipated losses for the new SG4 receiver design [4]. The 'outer aperture' plane, used for capture efficiency measurement, is at $x \approx -0.2$m, and the 'inner aperture', located at $x = 0$, is positioned at the location of peak flux.

SolarPACES 2016
AIP Conf. Proc. 1850, 110011-1–110011-8; doi: 10.1063/1.4984485
Published by AIP Publishing. 978-0-7354-1522-5/$30.00

FIGURE 2. The SG4 receiver, before insulation, and then installed and in operation. Peak temperatures observed are at the pipe restraints within the cavity.

best direct-tube-heating dish-Stirling receivers (Vanguard, MDAC) as reported by Stine and Diver [5], although it must be noted that these receivers were operating at 810°C, however the new receiver has now been built, installed and tested (Figure 2). Results presented in this paper demonstrate that an experimental receiver thermal efficiency of 97.1% was observed from approximately four hours of near-steady-state testing over several days (Table 1).

This paper details the experimental efforts at ANU to determine, as accurately as possible, the performance of the new receiver.

RECEIVER EFFICIENCY CALCULATION

In this paper we refer to two experimental measures of receiver efficiency. Receiver thermal-capture efficiency η is defined as the rate of internal heat transfer into the working fluid $\dot{Q}_I$ divided by the rate of radiative energy reflected by the dish $\dot{Q}_{\text{refl}}$. It incorporates the loss effects of receiver flux spillage, receiver reflections, thermal emissions from the cavity, external convection, and conduction. It is calculated from direct experimental measurements as follows:

$$\eta = \frac{\dot{Q}_I}{\dot{Q}_{\text{refl}}} = \frac{\dot{m}[h(p_o, T_o) - h(p_i, T_i)]}{\rho A_{\text{apert}} G} \tag{1}$$

where $\dot{m}$ is the receiver mass flow rate, h is the water/steam enthalpy calculated at the pressure p and temperature T_i of the inlet i or outlet o. On the numerator, ρ is the average solar-weighted mirror reflectance, A_{apert} is unshaded aperture area of the dish mirror surface, and G is the solar direct normal irradiance (DNI).

Receiver thermal efficiency η_{th} is similar, but includes only the loss effects of receiver reflection, thermal emissions, external convection, and conduction. It is related to the capture efficiency η_{capt} (also referred to as capture fraction [5]) as follows:

$$\eta_{\text{capt}} = \frac{\dot{Q}_{\text{inc}}}{\dot{Q}_{\text{refl}}} = 1 - \frac{\dot{Q}_{\text{spil}}}{\dot{Q}_{\text{refl}}} \text{ and } \eta_{\text{th}} = \frac{\dot{Q}_I}{\dot{Q}_{\text{inc}}} = \frac{\dot{Q}_I}{\dot{Q}_{\text{refl}} - \dot{Q}_{\text{spil}}} = \frac{\eta}{\eta_{\text{capt}}} \tag{2}$$

where $\dot{Q}_{\text{inc}}$ is the portion of the reflected radiative power which is incident upon the active surfaces of the receiver, and $\dot{Q}_{\text{spil}}$ is the remainder. Note that the thermal-capture efficiency η is not affected by changes in $\dot{Q}_{\text{spil}}$, but

TABLE 1. Summary of time-averaged experimental results for receiver efficiency (includes spillage, reflection, convection, re-radiation and conduction losses) and thermal efficiency (as above, but excludes spillage).

#	Date	Clock time	DNI	Reflectance	Inlet pressure	Wind speed	Outlet temperature	Thermal-capture efficiency	Thermal efficiency
			W/m²	%	bar	m/s	°C	%	%
1	18/11/15	11:35→12:54	1023±20	90.9±0.6	55.6±0.9	3.5±0.9	514±5	96.3±2.1	**97.2±2.2**
2	24/11/15	14:26→15:27	1035±21	92.9±0.6	57.2±0.9	3.1±0.9	509±5	95.8±2.1	**96.7±2.1**
3	04/12/15	10:34→11:32	1046±21	91.9±0.6	59.6±0.9	1.2±0.9	520±5	96.6±2.1	**97.5±2.2**
4	04/12/15	13:52→14:22	1052±21	91.9±0.6	57.7±0.9	1.8±0.9	558±5	96.1±2.1	**97.0±2.2**

η_{capt} and η_{th} are. The thermal-capture efficiency η defined in Eq. 1 was the basis of design optimisation in this project, since it incorporates all aspects of receiver design, especially the important trade-offs relating to aperture size, optical performance, and thermal losses.

In order to calculate an uncertainty for the resulting receiver efficiency, linear error propagation theory was used, with the aid of the Python `uncertainties` package [6]. This requires calculation of partial derivatives of water/steam enthalpy, which is achieved using routines from `freesteam` [7]. All measurements involve a combination of systematic and random errors [8], but in this study no attempt was made to separate random and systematic error sources, and all instrument and measurement errors were assumed to be systematic (implying that the uncertainty associated with each measurement does not reduce when values from a long time-series are averaged, as they would if they were random errors).

In the following section, the instrumentation for measuring receiver efficiency is described, with emphasis on the measurement uncertainty associated with each instrument.

MEASUREMENT AND UNCERTAINTY

Flow Rates, Pressures and Temperatures, and Wind Speed

The mass flow rate in the receiver is determined using a Yokogawa flow meter, positioned just before the feed-water pump, with a specified accuracy of ±0.35%. Flow rate measurements were cross-checked against an older E+H flow-meter and found to be in very good agreement.

Pressure measurement is via Yokogawa EJX530A pressure transducers located on the dish at the receiver inlet and outlet. These transducers were calibrated in late 2013, so according to the manufacturer data-sheet they are currently accurate to ±0.3% of span. The span was adjusted by Yokogawa to 300 bar, so at pressures of 50 bar, the error is ±0.9 bar. Data is converted from gauge to absolute pressure before being logged to the datafile, by addition of an assumed constant 1 bar atmospheric pressure.

Temperature measurement is via Type-K Class 2 thermocouples in thermal wells immersed in the inlet/outlet water/steam flow. The outlet thermocouple is connected for safety/control reasons to an analogue input on the dish programmable logic controller (PLC), a Yokogawa CU04-1S, while the inlet thermocouple is connected to the Yokogawa MW100 data logger. Accuracy of the thermocouples is taken as specified by IEC 60 584-2:1995, a tolerance of ±2.5 K for temperatures below 333°C, and a tolerance of $\pm 0.0075 \times T_{°\mathrm{C}}$ for temperatures 333–1200°C. The cold junction compensation in the CU04-1S is not specified by the manufacturer; it is assumed to add a further systematic uncertainty of ±2°C.

Wind speed is measured by two Monitor Systems AN2 anemometers which were calibrated to an accuracy ±2% of full-range (45 m/s). Wind speed is reported for completeness, due to its role in causing forced convection heat loss, but it is not a part of the calculation of η.

Dish Reflectance

The average solar-weighted mirror reflectance ρ for the dish must take account of the spectral reflectivity of the mirrors and their response to the solar spectrum at the time of the experiments, as well as the spatial variation across the dish surface due to variations in localised mirror soiling and potentially also in mirror quality.

Calibration of Portable Reflectometer

Measurement of the dish reflectance was via a portable Devices and Systems (D&S) 15R single-band specular reflectometer. This reflectometer was used with the largest aperture setting (46 mrad full-angle) to best approximate the acceptance angle of the dish (~1.5 m receiver outer aperture, ~13 m focal length).

In addition to its normal calibration process, the D&S 15R was further calibrated against a high-accuracy Varian Cary 5 UV-NIR spectrophotometer with 'VW' specular reflectance attachment. The full 'VW' calibration process was first followed, and then three mirror samples were carefully cleaned and their spectral specular reflectance $\rho_\lambda(\lambda)$ measured in the spectrophotometer (Figure 3). The spectrophotometer detection range was only 200–3000 nm, so the long-wavelength reflectivity of the mirrors had to be estimated from previous data. This value was estimated to be 40±10% for the range 3000–4000 nm. There is 0.83% of the total G173-03 energy in the 3000–4000 nm wavelength range.

When weighted against the ASTM G173-03 reference spectrum $G_\lambda(\lambda)$ according to Eq. 3, the measured mirror sample reflectance values were 94.41%, 94.40% and 94.33%. The spectrophotometer measurements for just first mirror sample were repeated three times and values were 94.41%, 94.41% and 94.40%, indicating minimal random error.

$$\overline{\rho}_{\text{sol}} = \frac{\int \rho_\lambda(\lambda) G_\lambda(\lambda) d\lambda}{\int G_\lambda(\lambda) d\lambda} \tag{3}$$

The same set of three mirrors was later measured with the D&S 15R. Each mirror was measured five times, and the largest standard error was found to be 0.06%. Averaged values $\rho_{\text{meas,D\&S}}$ for three mirrors were 96.26%, 96.08% and 96.16%.

The spectral sensitivity curve $\phi_\lambda(\lambda)$ for the D&S 15R was obtained from the instrument supplier, and an estimate of the expected 15R measurements $\rho_{\text{est,D\&S}}$ based on spectrophotometer readings was obtained according to Eq. 4. Expected values for the three mirrors were 96.21%, 96.28% and 96.11%. The discrepancy between the expected and measured values is within the ±0.2% repeatability value stated by the supplier

$$\rho_{\text{est,D\&S}} = \frac{\int \phi_\lambda(\lambda) \rho_\lambda(\lambda) d\lambda}{\int \phi_\lambda(\lambda) d\lambda} \tag{4}$$

The average value of the ratio $\overline{\rho}_{\text{sol}}/\rho_{\text{meas,D\&S}}$ was found to be 0.9811±0.0017, incorporating the effect of uncertain long-wave reflectance in the 3000–4000 nm range. This correction factor was used to estimate solar-weighted reflectance from the single-band measurements of the D&S 15R. Using the D&S 15R in this way implies 'grey' behaviour is being assumed for dust and soiling on the mirror, which appears reasonable for low levels of soiling [9] and also ignores possible variations in local solar spectrum from the standard ASTM G173-03. The impact of local changes in solar spectrum relative to the G173-03 standard has not yet been examined.

Averaging of Reflectivity Across the Dish Surfaces

Reflectivity of mirrors across the dish surface arises as a result of spatial variation in soiling and cleaning, as well as potentially variation in the quality of mirrors and variation in their rates of degradation over time. It is noticed that rain causes slight streaking of mirrors at times, although mirrors were thoroughly cleaned in advance of all of the tests here. Also, there is a rotating cleaning arm mounted on the dish which does not reach all the way to the dish edge, resulting in some systematic variation of reflectivity. The entire surface is cleaned manually with water and brushes in any case.

A large number of measurements (hundreds) were taken across the dish surfaces, and results were weighted to take into account systematic differences in reflectivity in different parts of the dish. An error analysis indicates a

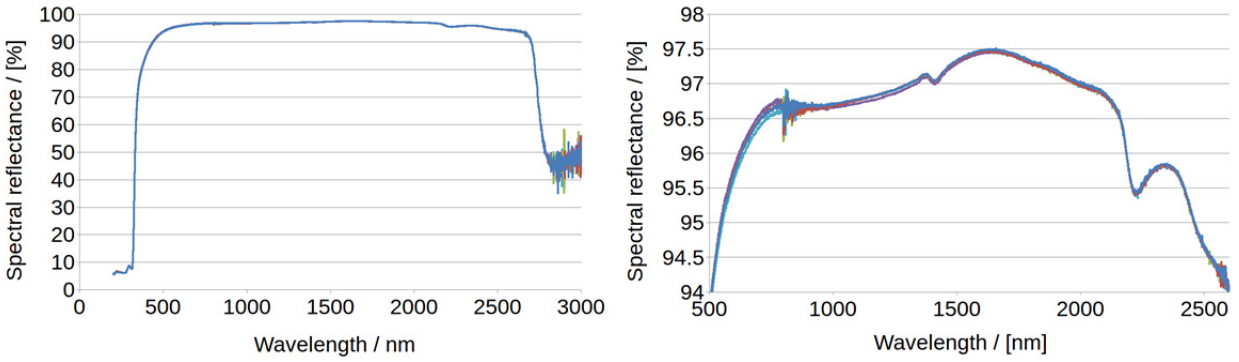

FIGURE 3. Spectrophotometer results for the three sample mirrors. Only very small variations are apparent between samples.

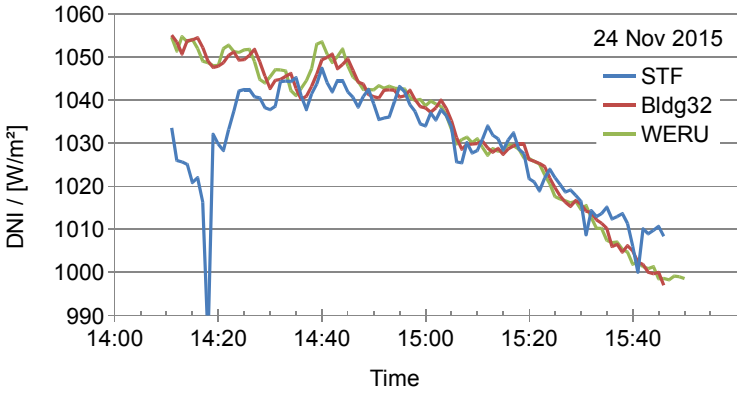

FIGURE 4. Good agreement on DNI measurements at two nearby locations was observed, suggesting that better than ±2% measurement accuracy is possible. The variation in the measured Solar Thermal Facility (STF) values early in the measurement period highlights the effect of incorrect (manual) pyrheliometer alignment, which was carefully monitored during the presented tests.

standard error from dish reflectivity measurement of no more than ±0.6% arose from the sampling, so this value of uncertainty was used as a conservative estimate.

Dish Aperture Area Measurement

The projected aperture of the mirrors on the SG4 dish is 489 m², which is reduced to 484.6 m² mostly due to shading from the receiver support trusses as well as a number of photogrammetry targets currently mounted on the mirrors. An uncertainty of 0.1% has been assigned to the aperture area to allow possible localised soiling of mirrors by the local cockatoo, galah and magpie populations, and this seems conservative.

Solar Direct Normal Irradiance Measurements

In this experiment, as with most CSP performance tests, the measurement of direct normal irradiance is critical, and one of the major sources of measurement uncertainty.

Measurement of the direct normal irradiance was via an Eppley Normal Incidence Pyrheliometer. The unit includes a simple mechanical tracking unit which requires occasional correction for drift. Although not recently calibrated the values from the pyrheliometer were cross-checked against a nearby unit at CSIRO Black Mountain as well as another pyrheliometer located on a nearby building at ANU (both ~1 km distance from the Big Dish).

Measurement uncertainty associated with the pyrheliometer was assumed to be ±2%, consistent with findings by NREL [10], and slightly wider than the ±1.5% assumed by Reinhalter et al [11]. Cross-checks between nearby sites suggest the error may be as low as ±0.6 or ±1.0% (Figure 4) but further investigation is required to assess this, and correlated errors between these 'independent' measurements may exist, for example temperature and zenith angle effects.

Flux Spillage and Peak Flux Measurement by Lunar Flux Mapping

The capture efficiency η_{capt} was determined from flux mapping of the full SG4 dish at night using the full moon. This method was previously used for flux mapping the SG3 dish [12] and then later the SG4 dish [13], where flux mapping was applied alongside full-dish photogrammetry, confirming reasonable agreement between ray-tracing and flux-mapping results for this dish. Since that time, however, a significant number of mirror panels on the SG4 dish have been replaced, and it was considered necessary to repeat the flux mapping. Lunar flux mapping also served to locate the focal plane of the dish before installation of the receiver.

Full-moon flux mapping was conducted on 28 Sept 2015 and 28 Oct 2015, and results were processed as follows. First, a raw flux-map image such as Figure 5 (left) is obtained. Background light levels are determined by examining the lowest pixel values from the regions near the corners of the image, and the background light (noise)

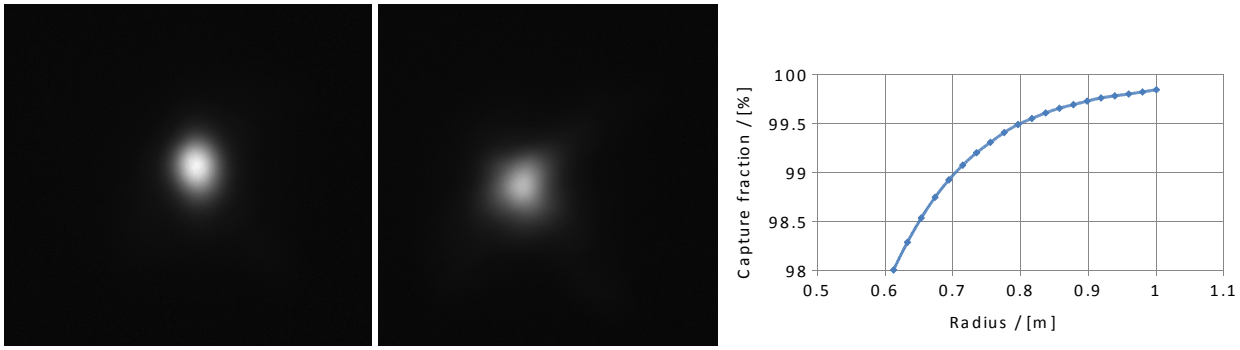

FIGURE 5. Flux mapping from 28 Sept 2015. Left, detail showing peak observed flux. Centre, detail showing flux at the receiver outer aperture plane, used for spillage calculation. Right, flux-in-radius plot for the outer aperture plane.

levels are subtracted from the whole image. Pixel values are then integrated to determine the total pixel value over the target plane. Then, based on DNI, aperture area and dish reflectivity, and assuming Lambertian reflection from the target, a conversion factor is established to convert pixel value into an aperture-plane incident flux distribution. A centroid is found, then radial binning is used to determine a flux-in-radius curve. Figure 5 (centre, right) shows the flux map and flux-in-radius curve for the outer aperture plane (as noted in Figure 1).

Flux maps were taken at a range of target positions in order to determine the location of the focal plane. Results showed that the focal length of the dish has increased slightly from 13.40 m to a current value of 13.43 m. This was cross-checked against whole-dish photogrammetry in Nov 2015, which gave a value of 13.42 m. Lengthening may be due to the mounting of additional safety-support members across the dish front surface (which were not intended to be structural, but which nevertheless may have stiffened the structure). Since the original SG4 flux mapping, the reported peak concentration of 14,000 suns [1] has also reduced to 11,000 suns (Figure 5 left); this may be explained by the slightly higher slope error of the more durable plywood-cored replacement mirror panels currently in use, compared to the original lower-cost panels.

The point on the flux-in-radius curve corresponding to the receiver outer aperture radius of 754 mm was used to determine the capture efficiency as η_{capt} =99.32%. This value was de-rated to 99.07% following an (approximate) analysis that suggested that 0.25% of flux was missing the flux target, based on the observation of flux profile in the corners of the image. As noted earlier, spillage does not affect values of η, but it does affect $\eta_{\text{th}} = \eta/\eta_{\text{capt}}$.

Time-Averaged Performance

Data was logged at two-second intervals over the full duration of testing. Periods were sought when the receiver temperature had reached its operating outlet temperatures of around 500°C. Reported periods include occasional manual adjustment of mass flow rate, in response to changing DNI. Analysis made use of the full two-second data set, with instantaneous efficiencies calculated and plotted, with uncertainties propagated throughout. Time averaged efficiencies and other parameters were then calculated from that time-series-with-uncertainty data.

RESULTS AND DISCUSSION

The test campaign for the big dish was run in Nov–Dec 2015 (late autumn/early summer), and resulted in four high-quality result sets where the dish operated at close to steady state for 30 minutes or more, with approximately four hours of two-second data altogether (Table 1). Across these four test periods, the receiver efficiency had an average of 96.2±2.1% and the receiver thermal efficiency had an average of 97.1±2.2%. A plot of the results for one test period is shown in Figure 6. Experimental uncertainty was dominated by the uncertainty in the DNI measurement. The relative impact of different measurement uncertainties is shown in Figure 7.

Although the average receiver thermal efficiency of 97.1±2.2% is consistent with the modelling prediction of 98.7% (the model is within the error bars), there are several possible explanations for the lower mean value. Firstly, modelling did not consider forced convection heat loss from the cavity. Secondly, modelling did not consider heat loss through the receiver support frame, and only considered the fibre insulation. Thirdly, modelling did not consider the small gap between tubes which was necessary for including the mounting straps; these gaps would decrease the active receiver area, increase outer-wall temperatures and increase losses. Fourthly, there were some differences in

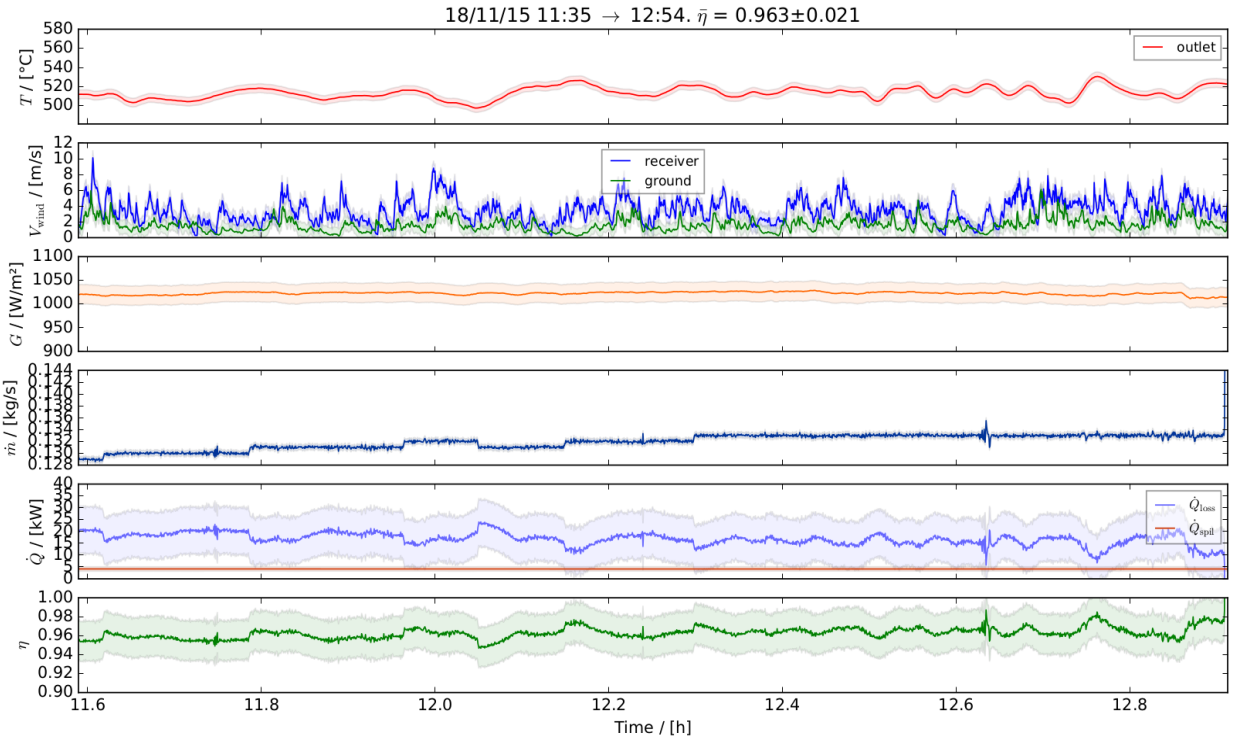

FIGURE 6. Results for the 79-minute test period starting 11:35 am on 18 Nov 2015. The average efficiency for this period was representative of other tests, and achieved 96.3±2.1%. Several manual adjustments to flow-rate were made in response to DNI and receiver temperature.

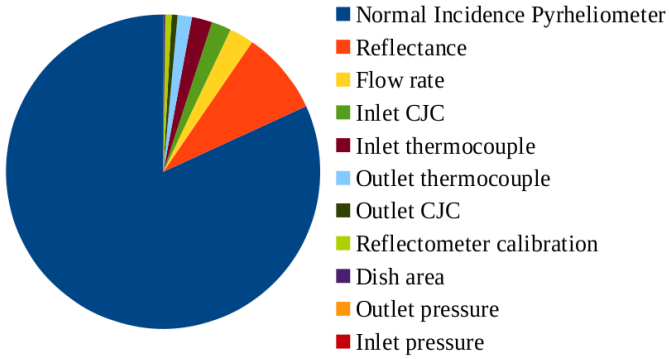

FIGURE 7. Propagation of measurement uncertainty to final receiver efficiency η. Graph shows contributions to total variance. The most significant uncertainty is seen to be the ±2% uncertainty in DNI measurement in the Eppley pyrheliometer. The next most significant uncertainty is the dish reflectance measurement, which is affected by local variations in reflectance due to soiling.

the observed and modelled temperature distributions on the outer aperture region (the 'pancake') which suggest that the simulated flux distribution did not accurately match reality; more flux on the pancake can be expected to increase losses. Finally, modelling was conducted without detailed treatment of the tube cross-section and tube external surface non-uniformity. Looking at the experiment as the source of error, the actual solar spectrum may not have been the same as the one used to determine the reflectometer compensation factor. Also, mass flow rates were changed manually from time to time during experiments, and so some transient effects might change the results.

There were some significant technical challenges arising during the tests. The very high concentration of the SG4 dish made getting on-sun and off-sun difficult, and in fact some receiver damage occurred, the assessment of which is the topic of some ongoing work. Also, the pump used to control the flow became unreliable and experimental flow rates could only be varied through quite a narrow band; testing with a wider range of flow rates and other conditions is desirable.

CONCLUSIONS

Across several tests, the average SG4 receiver thermal-capture efficiency was 96.2±2.1%, and the receiver thermal efficiency was 97.1±2.2%. The result compares favourably with the estimated 98.7% calculated from an integrated model at running at design conditions. The most likely cause of discrepancy is the presence of wind during the experiments, whereas wind was not considered in the modelling. The major source of experimental uncertainty is in the measurement of direct normal irradiance; some options exist to reduce this uncertainty with more rigorous calibration and/or compensation for temperature and zenith angle effects.

Although this receiver has a low operating temperature range of 60–500°C compared to the higher 810°C of previously Stirling engine receivers, the experimentally observed efficiency of 97.1% is a great improvement over the previous state of the art in Big Dish receivers, found through modelling to be 93.6% for the SG3 receiver on the SG3 dish [4]: total receiver thermal losses appear to have been more than halved.

Finally, it must be noted that a high-efficiency receiver can only be developed when the concentrator is of very high quality. The narrower aperture of the SG4 receiver compared to the SG3 receiver is a major reason for the large reduction in receiver losses, and highlights the importance of measuring the performance of the concentrator before finalising a receiver design.

ACKNOWLEDGEMENTS

Funding from the Australian Renewable Energy Agency (project 1-UFA006) is gratefully acknowledged.

Greg Burgess retired at the completion of this project. We thank him for his many years of fine contributions to the ANU Solar Thermal Group, and wish him all the best in his retirement.

We thank Cenk Kocer of the University of Sydney for use of the Varian Cary 5 UV-NIR spectrophotometer, as well as Steven Bosi for the aging but still useful video about its calibration and use.

Eric Lebigot's assistance in the use of his excellent `python-uncertainties` code is much appreciated.

REFERENCES

1. K. Lovegrove, G. Burgess and J. Pye (2011). *Sol. Energy* **85**, 620-626.
2. J. Cumpston and J. Pye (2015). *Solar Energy* **119**, 383-398.
3. G. Burgess, K. Lovegrove, S. Mackie, J. Zapata and J. Pye (2011). Direct steam generation using the SG4 500m² paraboloidal dish concentrator. In *Proceedings of SolarPACES 2011*, Granada, Spain.
4. J. Pye, G. Hughes, E. Abbasi-Shavazi, C.-A. Asselineau, G. Burgess, J. Coventry, W. Logie, F. Venn and J. Zapata (2015). Development of a Higher-Efficiency Tubular Cavity Receiver for Direct Steam Generation on a Dish Concentrator. In *SolarPACES 2015*, Cape Town.
5. W. B. Stine and R. B. Diver (1994). A compendium of solar dish/Stirling technology, Sandia Report SAND93-7026, Sandia National Laboratories, Alberquerque, NM.
6. Eric O. Lebigot, *'Uncertainties: a Python package for calculations with uncertainties'*, http://pythonhosted.org/uncertainties/. Accessed 24 Jul 2016.
7. John Pye, *'freesteam: Steam Tables, Open Source, IAPWS-IF97'*, http://freesteam.sourceforge.net/. Accessed 24 Jul 2016.
8. D. Kearney (2011). Utility-Scale Parabolic Trough Solar Systems: Performance Acceptance Test Guidelines, Subcontract report NREL/SR-5500-48895, NREL.
9. R. B. Pettit and J. M. Freese (1980). *Solar Energy Materials* **3**, 1-20.
10. D. R. Myers and S. M. Wilcox (2009). Relative Accuracy of 1-Minute and Daily Total Solar Radiation Data for 12 Global and 4 Direct Beam Solar Radiometers. In *American Solar Energy Society Annual Conference*, Buffalo, New York.
11. W. Reinalter, S. Ulmer, P. Heller, T. Rauch, J.-M. Gineste, A. Ferrière and F. Nepveu (2008). *Journal of Solar Energy Engineering* **130**, 011013.
12. P. Siangsukone, G. Burgess and K. Lovegrove (2004). Full Moon Flux Mapping the 400m² "Big Dish" at the Australian National University. In *Solar 2004: Life, the Universe, and Renewables*, Perth, Western Australia.
13. G. Burgess, J. Zapata, R. Chauvin, M. Shortis, J. Pye and J. Preston (2012). Three-dimensional flux prediction for a dish concentrator cavity receiver. In *Proceedings of SolarPACES 2012*, Marrakech, Morocco.